THESIS

DISENTANGLE MODEL DIFFERENCES AND FLUCTUATION EFFECTS IN DPD SIMULATIONS OF DIBLOCK COPOLYMERS

Submitted by

Paramvir Sandhu

Department of Chemical and Biological Engineering

In partial fulfillment of the requirements

For the Degree of Master of Science

Colorado State University

Fort Collins, Colorado

Spring 2013

Master's Committee:

Advisor: Qiang (David) Wang

Travis S. Bailey
Grzegorz Szamel

ABSTRACT

DISENTANGLE MODEL DIFFERENCES AND FLUCTUATION EFFECTS IN DPD SIMULATIONS OF DIBLOCK COPOLYMERS

In the widely used dissipative particle dynamics (DPD) simulations,[1] polymers are commonly modeled as discrete Gaussian chains interacting with soft, finite-range repulsions. In the original DPD simulations of microphase separation of diblock copolymer melts by Groot and Madden,[2] the simulation results were compared and found to be consistent with the phase diagram for the "standard model" of continuous Gaussian chains with Dirac δ-function interactions obtained from self-consistent field (SCF) calculations. Since SCF theory is a mean-field theory neglecting system fluctuations/correlations while DPD simulations fully incorporate such effects, the model differences are mixed with the fluctuation/correlation effects in their comparison. Here we report the SCF phase diagram for exactly the same model system as used in DPD simulations. Comparing our phase diagram with that for the standard model highlights the effects of chain discretization and finite-range interactions, while comparing our phase diagram with DPD simulation results unambiguously (without any parameter-fitting) reveal the effects of system fluctuations/correlations neglected in the SCF theory.

ACKNOWLEDGEMENTS

We thank Prof. Mark Matsen for providing us with his SCF results for the "standard" model. Financial support for this work was provided by the U.S. Department of Energy, Office of Basic Energy Sciences, Division of Materials Sciences and Engineering under Award DE-FG02-07ER46448. I thank my parents and sister for all the support and extra motivation they have given me.

TABLE OF CONTENTS

LIST OF TABLES

LIST OF FIGURES

Figure 7. Free energy per chain βf_c of various phases relative to the disordered phase obtained from our SCF calculations of the DPD model at $f = 0.3$

Figure 8. Free energy per chain βf_c of various phases relative to the disordered phase obtained from our SCF calculations of the DPD model at $f = 0.2$

Figure 9. Free energy per chain βf_c of various phases relative to the disordered phase obtained from our SCF calculations of the DPD model at $f = 0.1$

1 INTRODUCTION

Dissipative particle dynamics (DPD) is a coarse-grained dynamic simulation technique, which has been widely used in the literature since proposed by Hoogerbrugge and Koelman about 20 years ago.[1] In dimensional form, the total force acting on particle i in this method consists of three parts: $\mathbf{F}_i = \sum_{j\neq i}\left(\mathbf{F}_{ij}^C + \mathbf{F}_{ij}^D + \mathbf{F}_{ij}^R\right)$, where $\beta\sigma\mathbf{F}_{ij}^C = a_{ij}(1 - r_{ij}/\sigma)\hat{\mathbf{r}}_{ij}$ for $r_{ij} < \sigma$ and 0 otherwise is the conservative force applied by particle j on i, with $\beta \equiv 1/k_BT$, k_B being the Boltzmann constant, T the thermodynamic temperature, σ the cut-off radius, $a_{ij} \geq 0$ a dimensionless number controlling the interaction strength, $r_{ij} \equiv |\mathbf{r}_{ij}|$, $\mathbf{r}_{ij} \equiv \mathbf{r}_i - \mathbf{r}_j$, $\mathbf{r}_i$ denoting the spatial position of particle i, and $\hat{\mathbf{r}}_{ij} \equiv \mathbf{r}_{ij}/r_{ij}$; $\beta\sigma\mathbf{F}_{ij}^D = -\gamma\omega^D(r_{ij})\left[\hat{\mathbf{r}}_{ij}\cdot\sqrt{\beta m}(\mathbf{v}_i - \mathbf{v}_j)\right]\hat{\mathbf{r}}_{ij}$ is the dissipative (or drag) force, with $\gamma \geq 0$ being a dimensionless number controlling its strength, $\omega^D(r_{ij}) \geq 0$ a dimensionless weight function, m the particle mass (assumed to be the same for all particles), and $\mathbf{v}_i$ the velocity of particle i; and $\beta\sigma\mathbf{F}_{ij}^R = \alpha\omega^R(r_{ij})\xi_{ij}\hat{\mathbf{r}}_{ij}$ is the random force, with $\alpha \geq 0$ being a dimensionless number controlling its strength, $\omega^R(r_{ij}) \geq 0$ a dimensionless weight function, and ξ_{ij} a random number with zero mean and unit variance. One attractive feature of DPD simulation is that it conserves the momentum and thus gives the correct long-term hydrodynamic behavior of the system.[1]

In this work, however, we focus on the thermodynamic behavior. Espanol and Warren showed that, if $\alpha\omega^R(r_{ij}) = \sqrt{2\gamma\omega^D(r_{ij})}$, the Hamiltonian (or potential) for the conservative force $\beta\mathcal{H}^C$ then completely determines the system thermodynamics,[4] which means that such DPD simulations can in principle (1) sample the full spectrum of fluc-

tuations/correlations of the system, and (2) give the same thermodynamic properties as Monte Carlo (MC) simulations using $\beta\mathcal{H}^C$; the latter idea was indeed explored by Smit and co-workers.[5,6] We note that, as another attractive feature of DPD simulation, its $\beta\mathcal{H}^C$ is soft (i.e., allows complete particle overlapping). Using soft potentials is the basic idea of the so-called fast Monte Carlo (FMC) simulations,[7–9] which have recently attracted great interest especially in the study of polymeric systems.[10–15]

In particular, Groot and Madden first performed DPD simulations to study the microphase separation of linear diblock copolymer (DBC) A-B melts, and compared their results with those from the self-consistent field (SCF) calculations of Matsen and Bates;[16] after taking into account the fluctuation effects based on the theory of Fredrickson and Helfand (FH),[17] they found "quantitative match for the locations of the phase transitions".[2,18] Similar work was done by Chen et al.,[3] whose DPD results are consistent with and complementary to those of Groot and Madden. There are, however, several important differences between the DPD and SCF studies: First, the DPD simulations use a compressible system of discrete Gaussian chains (DGC) each of $N = 10$ segments interacting with a finite-range (DPD) potential, while the SCF calculations use the "standard" model, i.e., an incompressible system of continuous Gaussian chains (CGC) interacting with the Dirac δ-function potential. The system compressibility, chain discretization, and interaction range can all change the phase boundaries quantitatively. Second, SCF theory is a mean-field theory neglecting the system fluctuations/correlations. While such effects were taken into account by Groot and Madden based on FH theory, this theory is based on the Hartree analysis by Brazovskii[19] and the Ohta-Kawasaki effective Hamiltonian[20] for

the "standard" model. The Hartree analysis is rigorously accurate only for the invariant degree of polymerization $\bar{\mathcal{N}} \equiv (nR_{e,0}^3/V) \gtrsim 10^{10}$,[17] where n denotes the number of chains in volume V and $R_{e,0}$ the root-mean-square end-to-end distance of an ideal chain. As shown in Sec. 2.2.2 below, however, $\bar{\mathcal{N}} \approx 28$ and 77 in the DPD simulations, which do not justify the use of FH theory. Furthermore, the fitting of a_{ij} to the Flory-Huggins χ parameter characterizing the A-B repulsion in the "standard" model and the use of FH theory by Groot and Madden are not rigorous, as discussed in detail in Sec. 3.2.1.

Third, DPD is a dynamic simulation technique while SCF is an equilibrium approach, which means that the structure in DPD simulations could be kinetically trapped. Indeed, no well-ordered, spatially periodic structure was found in several cases of the DPD simulations,[2,3,18] as discussed in detail in Sec. 3.4. Fourth, a fixed-size box of $(20\sigma)^3$ with the periodic boundary conditions applied in all directions was used in the DPD simulations, which limits the allowed periods of the ordered structures,[21] but the SCF calculations minimize the system free energy by finding the bulk period of each ordered structure. While this is not a severe problem for the 1D lamellar structure due to the relatively large box size, it may be the main reason for obtaining the micellar phase in the DPD simulations[2,3,18] instead of the cylindrical phase predicted by SCF calculations. Last, Groot and Madden used binary blends of DBC with different compositions (volume fractions of the A-block in the copolymer) f to sample intermediate f-values that are not integer multiples of 0.1,[2,18] but the SCF calculations are for pure DBC systems. Comparisons between the DPD simulations and the SCF calculations of the "standard" model mix all these differences together; the meaning of "quantitative match" between the two is therefore not clear.

In this work, we perform both SCF calculations and FMC simulations in a canonical ensemble based on exactly the same model DBC system as used in the DPD simulations (i.e., $\beta\mathcal{H}^C$ including the bonding potential)[2,3]. In particular, in addition to the cubic box of $(20\sigma)^3$, our FMC simulations are also performed in variable-length boxes to find the bulk period of lamellar and cylindrical structures. Comparing our SCF results with those for the "standard" model therefore unambiguously reveals the effects of model differences (i.e., the system compressibility, chain discretization, and interaction range), and comparing our SCF and FMC results reveals, without any parameter-fitting, the effects of system fluctuations/correlations neglected in the SCF theory. Furthermore, comparing our fixed-box FMC results with the DPD results unambiguously identifies the kinetically trapped structures in the latter, and comparing our SCF (or FMC) results in both fixed- and variable-length boxes unambiguously reveals the effects of fixed vs. bulk periods. For simplicity, we only consider systems of pure DBC in this work.

2 MODEL AND METHODS

The discrete Gaussian chain (DGC) model is first introduced in Sec. 2.1 for a single homopolymer chain. In Sec. 2.2.2, this model will be extended to a system of many chains using the DPD potential. We give a brief description of MC simulations done by Jing Zong in our research group. In Sec. 2.4 we derive field theory from a particle model for homopolymers. Finally in Sec. 2.5, we develop the SCFT for diblock copolymers using the DPD model.

2.1 DISCRETE GAUSSIAN CHAIN MODEL

The DGC model is a type of bead-and-spring model in which the coarse-grained particles along a polymer chain are treated as beads that are jointed by "spring potentials". Assuming all N bonds of a DGC chain are equal, the bonding potential energy of a single ideal (only short-ranged interactions) homopolymer chain can be given as

$$\beta u^b = \frac{3}{2a^2} \sum_{s=1}^{N} |\mathbf{b}_s| \tag{1}$$

where $\mathbf{b}_s = \mathbf{R}_s - \mathbf{R}_{s-1}$ is the bond vector between particle $s-1$ and s, and $a = |\mathbf{b_s}|$ is the effective bond length. The single chain partition function is then given by

$$\mathcal{Z} = V \left(\int \mathrm{d}\mathbf{R} \exp\left\{ -\beta u^b \right\} \right)^N \tag{2}$$

One means by which the statistical properties of chain models can be studied is through inspection of the normalized reduced probability distribution function, $p_0(\mathbf{r}, s)$. $p_0(\mathbf{r}, s)$ is

the probability density that a polymer chain consisting of $s+1$ particles has its end, s, at position $\mathbf{r}$.[22] Typically, we make an initial guess of the probability density for the end position of a chain with one particle fewer, $p_0(\mathbf{r}, s-1)$. This guess allows us to build up a chain consisting of $s+1$ particles by adding a particle and a bond to the s-particle chain. There is an additional probability associated with the addition and bonding of a new particle called the bond transition probability, $\Phi(\mathbf{b_s}; \mathbf{R}_{s-1})$. This probability is associated with orientation of the added bond. In particular, it represents the probability density that the added bond connecting particles s and $s-1$ has a value of $\mathbf{b_s}$ if particle $s-1$ is located at position $\mathbf{R}_{s-1}$.[22] Once the bond transition probability is known for a specific model, we can determine $p_0(\mathbf{r}, s)$ by

$$p_0(\mathbf{r}, s) = \int \mathrm{d}\mathbf{b_s} \Phi(\mathbf{b_s}; \mathbf{R}_{s-1}) p_0(\mathbf{R}_{s-1}, s-1) \tag{3}$$

This equation is known as a Chapman-Kolmogorov equation (CKE) in the theory of stochastic processes. Note that Eq. (3) is a three-dimensional convolution integral that can be solved by Fourier transform. The normalized bond "transition" probability for the DGC model is

$$\Phi(\mathbf{b_s}; \mathbf{R}_{s-1}) = \Phi(\mathbf{b_s}) = \frac{\exp[-\beta u^b]}{\int \mathrm{d}\mathbf{b_s} \exp[-\beta u^b]} = \left(\frac{3}{2\pi a^2}\right)^{d/2} \exp\left(\frac{3|\mathbf{b_s}|^2}{2a^2}\right) \tag{4}$$

which signifies the Gaussian distribution of bond displacements.[22] $\mathbf{b_s}$ denotes the bond vector of the s^{th} and $(s-1)^{\text{th}}$ segments. The convenience of the DGC model arises from carrying out analytical calculations that are made possible by the Gaussian description of segments at both the level of a coarse-grained bond and the level of the end-to-end vector.[22]

In contrast to the "standard model", DBCs are modeled by a continuous Gaussian chain (CGC) where the location of each segment on the polymer chain backbone is parameterized by a contour variable s that increases from 0 to 1. The bonded potential energy βu^b of the CGC can be written as a functional of the space curve $\mathbf{r}(s)$ that defines the configuration of the polymer, and is given as

$$\beta u^b[\mathbf{r}] = \frac{3}{2a^2}\int_0^N \mathrm{d}s \left[\frac{\mathrm{d}\mathbf{r}(s)}{\mathrm{d}s}\right]^2 \tag{5}$$

The CGC model is the continuum limit of the DGC model corresponding to $N \to \infty$.

2.2 DISSIPATIVE PARTICLE DYNAMICS

2.2.1 MONOMERIC FLUIDS

Before developing a field theory model for diblocks, we must first determine the potentials used in the particle-based DPD model in order to make an exact comparison to study system fluctuations. Dissipative particle dynamics is a type of particle based mesoscopic simulation method in which atoms of a polymer melt are grouped into particles. These particles act as centers of mass whose motion is governed by certain collision rules. The particles are modeled as bead-and-spring type soft spheres.[23] Hoogerbrugge and Koelman[1] first introduced DPD and defined three forces that particles experience in DPD simulations: a soft repulsive interaction force $\mathbf{F}^C$ called the conservative force, a dissipative or friction force $\mathbf{F}^D$, and a random force $\mathbf{F}^R$. The random force defines the random collisions with solvent molecules and the dissipative force results from the drag of the polymer chain. The

dissipative and random forces need to satisfy a specific relationship to preserve the statistical mechanics of the system in the canonical ensemble (N,V,T).[4] The model system used in Ref. [2] gives the conservative force as

$$\beta\sigma\mathbf{F}_{ij}^{C} = \begin{cases} a_{ij}\left(1-\frac{r_{ij}}{\sigma}\right)\hat{\mathbf{r}}_{ij} & \text{if } r_{ij} < \sigma \\ 0 & \text{otherwise} \end{cases} \tag{6}$$

where i, j are particle indices, a_{ij} is the maximum repulsion between particles i and j, $\beta = 1/k_B T$, σ is cutoff radius, $\mathbf{r}_{ij} = \mathbf{r}_i - \mathbf{r}_j$, $r_{ij} = |\mathbf{r}_{ij}|$, and $\hat{\mathbf{r}}_{ij} = \mathbf{r}_{ij}/r_{ij}$. The dissipative and random forces are given by

$$\mathbf{F}_{ij}^{D} = -\gamma w^{D}(r_{ij})\hat{\mathbf{r}}_{ij}\cdot(\mathbf{v}_i - \mathbf{v}_j)\hat{\mathbf{r}}_{ij}, \;\; \mathbf{F}_{ij}^{R} = \alpha w^{R}(r_{ij})\zeta_{ij}\hat{\mathbf{r}}_{ij}, \tag{7}$$

where w^D and w^R are weight functions that are zero for $r > r_c$, $\zeta_{ij}(t)$ is a random variable with zero mean and unit variance.[2] Espanol and Warren[4] showed that if the dissipative and random forces satisfy the following relations,

$$\begin{cases} w^{D}(r_{ij}) = [w^{R}(r_{ij})]^2 \\ \gamma = \beta\alpha^2/2 \end{cases}$$

the Hamiltonian (or potential) for the conservative force completely determines the thermodynamics of the system. The above relations along with their respective forces act as the thermostat of the system corresponding to the canonical ensemble. The reader is referred to Refs.[1, 2, 4, 23] for detailed derivation and explanation of DPD simulations.

2.2.2 DIBLOCK COPOLYMERS

The remaining focus is on the conservative potential for compressible diblock copolymer melts, first used by Groot and Madden in 1998.[2] The model system used in Ref. [2] consists of n DBC chains, each having N_{A} segments of type A followed by N_{B} segments of B. In Ref. [2], the volume fraction of the A block in the copolymer is given as $f \equiv N_{\mathrm{A}}/N$ with $N \equiv N_{\mathrm{A}} + N_{\mathrm{B}} = 10$. To describe chain connectivity, Groot and Madden[2] define the bonded force as a Harmonic spring potential given as

$$\beta\sigma\mathbf{F}_{ij}^{S} = \frac{-4\mathbf{r}_{ij}}{\sigma} \tag{8}$$

between two connected segments i and j, where σ denotes the cut-off radius (set to 1 in Ref. [2]), $\mathbf{F}_{ij}^{S}$ is the force acting by segment j on i, and $\mathbf{r}_{ij} \equiv \mathbf{r}_i - \mathbf{r}_j$ where $\mathbf{r}_i$ is the spatial position of segment i.

In terms of a potential, we arrive at the discrete Gaussian chain (DGC) model for the chain connectivity; that is, adjacent segments on a chain are connected by Gaussian springs with a bonding potential

$$\beta u_{k,s}^{b} = \frac{3}{2a^2}\left(\mathbf{R}_{k,s+1} - \mathbf{R}_{k,s}\right)^2 \tag{9}$$

where $\beta \equiv 1/k_B T$, a denotes the effective bond length, and $\mathbf{R}_{k,s}$ denotes the spatial position of the s^{th} segment on the k^{th} chain. Comparing the above with the spring force $\beta\sigma\mathbf{F}_{ij}^{S}$, we find that $\sigma/a = 2/\sqrt{3}$ (i.e., $R_{e,0} \equiv \sqrt{N-1}a = 3\sqrt{3}\sigma/2$) is used in Ref. [2]. It can be easily

seen by comparing this potential with that given by Eq. (13) that the chains are indeed modeled as DGCs. Thus the Hamiltonian of the bonded potential is written as

$$\beta H^b = \frac{3}{2a^2} \sum_{k=1}^{n} \sum_{s=1}^{N-1} \left(\mathbf{R}_{k,s+1} - \mathbf{R}_{k,s}\right)^2 \tag{10}$$

Note that Eq. (6), is actually the non-bonded force including forces between A-A, B-B, and A-B segments. This force can be written in terms of two potentials: All segments regardless of their type) interact with a pair potential

$$u^{\kappa}(r) = \frac{u_0(r)}{\kappa \rho_0}$$

where r denotes the distance between two segments, the pair potential $\beta u_0(r) = (15/2\pi\sigma^3)(1 - r/\sigma)^2$ for $r < \sigma$ and 0 otherwise (note that the coefficient here is chosen such that the DPD potential $\beta u_0(r)$ is normalized in 3D, i.e., $\int \mathrm{d}\mathbf{r} \beta u_0(r) = 1$; in the limit of $\sigma \to 0$, $\beta u_0(r)$ then becomes the Dirac δ-function potential $\delta(r)$), the average segmental number density $\rho_0 \equiv nN/V$ with V being the system volume, and the generalized Helfand compressibility[24,25] $\kappa \geq 0$ controls the interaction strength ($\kappa = 0$ corresponds to the hard-sphere chains).

In addition, an A segment interacts with a B segment via a pair potential

$$u^{\chi}(r) = u_0(r)\chi/\rho_0$$

with the generalized Flory-Huggins parameter $\chi \geq 0$ controlling the A-B repulsion strength. Comparing these pair potentials with the conservative force given by Eq. (2) of Ref. [2] or

Eq. (6), we find that the maximum repulsion parameters used in Ref. [2] are given by

$$\begin{cases} a_{AA} = a_{BB} = \frac{15}{\pi\sigma^3}\frac{1}{\kappa\rho_0} \\ a_{AB} = \frac{15}{\pi\sigma^3}(\frac{1}{\kappa\rho_0} + \frac{\chi}{\kappa\rho_0}) \end{cases} \tag{11}$$

Their value of $a_{\mathrm{AA}} = a_{\mathrm{BB}} = 75/\rho_0\sigma^3$ therefore corresponds to $N/\kappa = 50\pi$. In addition, the two segmental densities, $\rho_0\sigma^3 = 3$ and 5, used in Ref. [2] correspond to the invariant degree of polymerization $\bar{\mathcal{N}} \equiv (nR_{e,0}^3/V)^2 \approx 28$ and 77, respectively. Their value of $a_{\mathrm{AB}} = 40$ used at $\rho_0\sigma^3 = 3$ corresponds to $\chi N = 30\pi$, and $a_{\mathrm{AB}} = 21$ used at $\rho_0\sigma^3 = 5$ corresponds to $\chi N = 20\pi$. The Hamiltonian for the non-bonded potentials can be written as a sum of the different pair potentials given as

$$H^{nb} = \frac{1}{\kappa\rho_0}\sum_{i\in A, j\in A, i<j} u_0(r_{ij}) + \frac{1}{\kappa\rho_0}\sum_{i\in B, j\in B, i<j} u_0(r_{ij}) + \left(\frac{1}{\kappa\rho_0} + \frac{\chi}{\rho_0}\right)\sum_{i\in A, j\in B} u_0(r_{ij}) \tag{12}$$

The total Hamiltonian for the conservative potential can be written as a sum of the bonded and non-bonded potentials

$$H^C = H^b + H^{nb}$$

We now have a complete effective mapping between Groot and Madden's DPD model[2] given by Eq. (6) and Eq. (8) to our model defined by Eq. (10) and Eq. (12). After normalizing all lengths by $R_{e,0}$, we have totally six parameters: N, σ/a, $f = N_A/N$, N/κ, χN, and $\bar{\mathcal{N}}$. The first two are model parameters characterizing the chain discretization and interaction range, respectively, and the rest are physical parameters that can be mapped to an experimental system. In particular, f denotes the volume fraction of the A block, κ the system compress-

ibility, χ the A-B incompatibility, and $\bar{\mathcal{N}}$ the so-called invariant degree of polymerization controlling the system fluctuations. It's essentially the number of chains with which a single chain interacts within its volume; when $\bar{\mathcal{N}}$ is large, a chain interacts with many other chains and the system fluctuations are small.

2.3 FAST-OFF LATTICE MONTE CARLO SIMULATIONS

To study and quantify system fluctuations, the DPD model presented in Secs. 2.2.1, 2.2.2 was used to perform Fast-Off Lattice Monte Carlos (FOMC) simulations, and the results were compared with the SCFT calculations for the same Hamiltonian without any parameter fitting. FOMC is a particle based simulation technique where excluded-volume interactions are modeled by "soft" repulsive potentials that allow particle overlapping.[7] The main idea is to prevent the use of hard repulsions, such as the commonly used Lennard-Jones potential, to allow faster chain relaxation and better sampling to study equilibrium properties of soft materials. And since polymers are typically modeled by soft potentials consisting of volumeless segments with the excluded-volume interactions described by the Helfand compressibility,[7] FOMC provides an excellent tool to apply our DPD model to study the effects of fluctuations in diblock copolymers.

We perform FOMC simulations of the above model system in a canonical ensemble with trial moves of hopping,[7] reptation,[7] pivot,[26] and box-length change (when a rectangular parallelepipedal simulation box with variable lengths is used). For pivot moves, we randomly rotate the shorter portion of a randomly chosen chain around a segment,[26]

instead of a bond as in the original pivot algorithm.[27] Note that the highly efficient pivot trial moves cannot be used in many-chain simulations with hard excluded-volume interactions (e.g., the Lennard-Jones potential or the self- and mutual-avoiding walk on a lattice) due to their extremely small acceptance rates;[28] with soft potentials, however, we achieve acceptance rates of more than 50% here.[26] More details are given in Ref. [26].

In simulations of periodic structures, the periodic boundary conditions limit the allowed orientations of the structure and thus its period. For example, for lamellae with a normal direction $\mathbf{n}$ in a simulation box with length L_j in the $\mathbf{j}(= \mathbf{x}, \mathbf{y}, \mathbf{z})$ direction, $L_j \mathbf{j} \cdot \mathbf{n} = n_j L(\mathbf{n})$ must be satisfied, where n_j is the number of periods contained in the box along the $\mathbf{j}$ direction (which could be 0) and L the lamellar period; this gives $L(\mathbf{n}) = 1 \Big/ \sqrt{\sum_{\mathbf{j}} (n_j/L_j)^2}$.[21] For a fixed-length box as commonly used in canonical-ensemble simulations, both the lamellar orientation and its period are therefore discretized (i.e., L can hardly be L_0).[21] To eliminate this problem for lamellar structures, we use box-length change trial moves to generate, without loss of generality, the new box length along the x direction as $L_{x,\text{new}} = L_{x,\text{old}} \exp(\xi)$, where $L_{x,\text{old}}$ is the box length before the trial move and ξ a random number uniformly distributed within $(-\xi_{\max}, \xi_{\max})$, and set the box lengths along the other two directions to be the same (i.e., $L_y = L_z$), which are varied accordingly to keep V constant. The spatial positions of all segments are then re-scaled in each direction.[26] For 2D hexagonally packed cylindrical structures, where the restriction of a fixed-length box is more severe,[29] we use similar trial moves except keeping $L_y = \sqrt{3} L_z$. We have not performed FOMC simulations of 3D periodic structures, where canonical-ensemble simulations at a fixed V cannot be used to find the bulk period.

Finally, to determine the order-disorder transition (ODT) of symmetric DBC, we use replica-exchange[30] at different χN (with acceptance rates of 50∼80%) to further improve our sampling, a new order parameter characterizing the degree of positional order in lamellae, and multiple histogram reweighting[31] to accurately locate ODT according to the equal-weight criterion.[32] More details are given in Ref. [26].

All FMC simulations were performed by Jing Zong in our research group.

2.4 PARTICLES TO FIELDS: HOMOPOLYMERS

We will now extend our discussion to a system of many homopolymer chains in a spatially varying chemical potential field $\omega(\mathbf{r})$ which acts on all s segments on k chains. Once the particle to field transformation is understood for a system of homopolymer chains, the formalism can easily be applied to diblock copolymers. In a system of many chains, adjacent segments on a chain modeled as DGCs interact with a bonding potential given as

$$\beta u^b = \frac{3}{2a^2} \sum_{k=1}^{n} \sum_{s=1}^{N-1} \left(\mathbf{R}_{k,s+1} - \mathbf{R}_{k,s}\right)^2 \tag{13}$$

where $\mathbf{R}_{k,s}$ denotes the spatial position of the s^{th} segment on the k^{th} chain for N segments and n chains. Note this equation differs only by the summations in comparison to the single chain potential given by Eq. (1), and $\mathbf{R}_{k,s+1} - \mathbf{R}_{k,s}$ is the equivalent bond vector. All

non-bonded segments interact with a pair potential that we will define as

$$\beta u^{nb}(r_{i,j}) = \frac{1}{2}\sum_{i=1}^{nN}\sum_{j=1(\neq i)}^{nN} u_0(r_{ij}) \tag{14}$$

where $r_{i,j} = |\mathbf{r}_{ij}|$, $|\mathbf{r}_{ij}| = \mathbf{r}_i - \mathbf{r}_j$, and $u_0(r_{ij})$ is an arbitrary pair potential function. The factor of $(1/2)$ is a correction for the double counting of each particle pair twice.

The potential is first written in terms of microscopic particle density which is a sum of Dirac δ-functions of the coordinates of each atom

$$\hat{\rho}(\mathbf{r}) = \sum_{k=1}^{n}\sum_{s=1}^{N}\delta(\mathbf{r} - \mathbf{R}_{k,s}) \tag{15}$$

The non-bonded potential can be redefined as

$$\beta u^{nb}(r_{i,j}) = \frac{1}{2}\int \mathrm{d}\mathbf{r}\int \mathrm{d}\mathbf{r}'\hat{\rho}(\mathbf{r})u_0(|\mathbf{r}-\mathbf{r}'|)\hat{\rho}(\mathbf{r}') - \frac{nN}{2}u_0(0) \tag{16}$$

where the last term deducts the self-interactions. The configurational canonical-ensemble partition function can we written as

$$\mathcal{Z} = A_0^n \prod_{k=1}^{n}\sum_{s=1}^{N}\int \mathrm{d}\mathbf{R}_{k,s}\exp\left[-\sum_{k=1}^{n}\sum_{s=1}^{N-1}\beta u_{k,s}^b - \frac{1}{2}\int \mathrm{d}\mathbf{r}\int \mathrm{d}\mathbf{r}'\hat{\rho}(\mathbf{r})u_0(|\mathbf{r}-\mathbf{r}'|)\hat{\rho}(\mathbf{r}')\right] \tag{17}$$

where the constant $A_0 = \exp\left(\frac{nN}{2}\beta u_0(0)\right)/n!$. The definition of the delta functional, or the Hubbard-Stratonovich transformations, is also used in the particle-to-field transformation and is defined as $\int \mathscr{D}\rho\delta[\rho - \hat{\rho}] = F[\hat{\rho}]$ for any functional $F[\rho]$. An "infinite-dimensional"

Dirac delta function is a delta functional $\delta[\rho - \hat{\rho}]$ that vanishes for all positions $\mathbf{r}$ except where the fields $\rho_j(\mathbf{r})$ and $\hat{\rho}_j(\mathbf{r})$ are equal. To transform the above particle model to a field model, we make use of techniques related to the Hubbard-Stratonovich transformations in which the interactions between polymer segments are decomposed and essentially replaced by interactions between the segments and conjugate fields.[22] This is done by inserting in Eq. (17) the following identity

$$1 = \int \mathscr{D}\phi \mathscr{D}\omega \exp\left(\int \mathrm{d}\mathbf{r} \omega(\mathbf{r})[\rho_0 \phi(\mathbf{r}) - \hat{\rho}(\mathbf{r})] \right) \tag{18}$$

where $\phi(\mathbf{r})$ is a normalized density field constrained to $\hat{\rho}(\mathbf{r})/\rho_0$ and $\omega(\mathbf{r})$ is a purely imaginary conjugate field interacting with all segments that imposes the constraint. Inserting this identity in Eq. (17) we obtain

$$\begin{aligned} \mathcal{Z} &= A_0^n \prod_{k=1}^{n} \sum_{s=1}^{N} \int \mathscr{D}\phi \mathscr{D}\omega \int \mathrm{d}\mathbf{R}_{k,s} \exp(\eta) \\ \eta &= -\sum_{k=1}^{n} \sum_{s=1}^{N-1} \beta u_{k,s}^b - \frac{1}{2} \int \mathrm{d}\mathbf{r} \int \mathrm{d}\mathbf{r}' \hat{\rho}(\mathbf{r}) u_0(|\mathbf{r} - \mathbf{r}'|) \hat{\rho}(\mathbf{r}') + \int \mathrm{d}\mathbf{r} \omega(\mathbf{r})[\rho_0 \phi(\mathbf{r}) - \hat{\rho}(\mathbf{r})] \end{aligned} \tag{19}$$

Some mathematical manipulations can be made to arrive at a more functional form. First, the n particle position integrals can be factored and the integral is raised to the power n. We further re-scale variables according to $\mathbf{r}/R_{e,0} \to \mathbf{r}$ (thus $V/R_{e,0}^d \to V$, where $R_{e,0} = \sqrt{N-1}a$ and d is the number of dimensions in which calculations are performed), $u_0(|\mathbf{r} - \mathbf{r}'|)R_{e,0}^d \to u_0(|\mathbf{r} - \mathbf{r}'|)$, and $N\omega(\mathbf{r}) \to \omega(\mathbf{r})$. After some manipulations we obtain

$$\mathcal{Z} = \int \mathscr{D}\phi \mathscr{D}\omega \exp\{-n\beta f_c[\phi, \omega]\}$$

with

$$\beta f_c = \frac{1}{2V}\int \mathrm{d}\mathbf{r}\int \mathrm{d}\mathbf{r}'\,[\phi(\mathbf{r})]\,u_0(|\mathbf{r}-\mathbf{r}'|)\phi(\mathbf{r}') - \frac{1}{V}\int \mathrm{d}\mathbf{r}\omega(\mathbf{r})\phi(\mathbf{r}) - \ln Q[\omega] \tag{20}$$

where the Stirling approximation $\ln n! \approx n\ln n - n$ is used, a constant factor is omitted in $\mathcal{Z}$, and the single-chain partition function is defined as $Q \equiv \prod_{s=1}^{N}\int d\mathbf{R}_s \cdot \exp\left[-\sum_{s=1}^{N-1}\beta u_s^b - \sum_{s=1}^{N}\omega(\mathbf{R}_s)/N\right]\Big/G$ with $G \equiv \prod_{s=1}^{N}\int d\mathbf{R}_s \cdot \exp\left(-\sum_{s=1}^{N-1}\beta u_s^b\right)$. The partition function can be rewritten in by recalling the definition of the normalized transition probability, Eq. (4). Furthermore, after applying the definition of the normalized transition probability, the partition function can be further expressed by a functional known as the chain propagator defined as

$$q_{s+1}(\mathbf{r}) = \exp[-\omega(\mathbf{r})]\int \mathrm{d}\mathbf{r}'\Phi(|\mathbf{r}-\mathbf{r}'|)q_s(\mathbf{r}') \tag{21}$$

which is a Chapman-Kolmogorov equation analogous to the probability density given by Eq. (3) for the particle case. The chain propagator can be built up recursively by starting with the initial condition $q_0(\mathbf{r}) = 1$. The chain propagator, $q_s(\mathbf{r})$, is the statistical weight for a chain of $s+1$ beads to have its end at position $\mathbf{r}$.[22] The reason we are interested in this functional for single chains is because once the mean-field (or SCFT) approximation is applied, the problem of many chains reduces to that of a single noninteracting polymer chain in external fields.

2.5 DIBLOCK COPOLYMERS: SELF-CONSISTENT FIELD (SCF) THEORY

Now that we have forms of potentials for DGC diblock copolymers, we can develop the field theory as done for homopolymers in Section 2.2. We begin by identifying the configurational canonical-ensemble partition function of the system as

$$\mathcal{Z} = \prod_{k=1}^{n} \sum_{s=1}^{N} \int \mathrm{d}\mathbf{R}_{k,s} \cdot \exp\left\{ -\sum_{k=1}^{n} \sum_{s=1}^{N-1} \beta u_{k,s}^{b} - \beta \mathcal{H}^{nb}[\hat{\rho}_{\mathrm{A}}, \hat{\rho}_{\mathrm{B}}] \right\} \tag{22}$$

where we have written the non-bonded Hamiltonian in terms of microscopic densities of A and B segments defined as $\hat{\rho}_{\mathrm{A}}(\mathbf{r}) \equiv \sum_{k=1}^{n} \sum_{s=1}^{N_{\mathrm{A}}} \delta(\mathbf{r}-\mathbf{R}_{k,s})$ and $\hat{\rho}_{\mathrm{B}}(\mathbf{r}) \equiv \sum_{k=1}^{n} \sum_{s=N_{\mathrm{A}}+1}^{N} \delta(\mathbf{r}-\mathbf{R}_{k,s})$, respectively at spatial position $\mathbf{r}$. The Hamiltonian due to non-bonded interactions is given by

$$\begin{aligned} \mathcal{H}^{nb} = & \frac{1}{2\kappa\rho_0} \int \mathrm{d}\mathbf{r}\mathrm{d}\mathbf{r}' \left[\hat{\rho}_{\mathrm{A}}(\mathbf{r}) + \hat{\rho}_{\mathrm{B}}(\mathbf{r})\right] u_0(|\mathbf{r}-\mathbf{r}'|) \left[\hat{\rho}_{\mathrm{A}}(\mathbf{r}') + \hat{\rho}_{\mathrm{B}}(\mathbf{r}')\right] - \frac{nN}{2\kappa\rho_0} u_0(0) \\ & + \frac{\chi}{\rho_0} \int \mathrm{d}\mathbf{r}\mathrm{d}\mathbf{r}' \hat{\rho}_{\mathrm{A}}(\mathbf{r}) u_0(|\mathbf{r}-\mathbf{r}'|) \hat{\rho}_{\mathrm{B}}(\mathbf{r}') \end{aligned} \tag{23}$$

Note that Eq. (23) is simply the summation of $u^{\kappa}(r)$ and $u^{\chi}(r)$ over all segment pairs in the system. We note that Eq. (23) is equivalent to Eq. (A4) in our previous work, Ref. [7]. Next, we can transform the above particle-based model to a field-based one following the methodology in Section 2.2 by inserting in Eq. (22) the following identity.

$$1 = \prod_{j=\mathrm{A,B}} \int \mathscr{D}\phi_j \mathscr{D}\omega_j \exp\left\{ \int \mathrm{d}\mathbf{r} \omega_j(\mathbf{r}) \left[\rho_0 \phi_j(\mathbf{r}) - \hat{\rho}_j(\mathbf{r})\right] \right\}$$

where $\phi_{\rm A}(\mathbf{r})$ and $\phi_{\rm B}(\mathbf{r})$ are normalized segmental density (volume fraction) fields constrained to $\hat{\rho}_{\rm A}(\mathbf{r})/\rho_0$ and $\hat{\rho}_{\rm B}(\mathbf{r})/\rho_0$, respectively, and $\omega_{\rm A}(\mathbf{r})$ and $\omega_{\rm B}(\mathbf{r})$ are (purely imaginary) conjugate fields interacting with A and B segments, respectively, which impose the constraints. We further re-scale variables according to $\mathbf{r}/R_{e,0} \to \mathbf{r}$ (thus $V/R_{e,0}^d \to V$, where $R_{e,0} = \sqrt{N-1}a$ and d is the number of dimensions in which calculations are performed), $u_0(|\mathbf{r}-\mathbf{r}'|)R_{e,0}^d \to u_0(|\mathbf{r}-\mathbf{r}'|)$, and $N\omega_j(\mathbf{r}) \to \omega_j(\mathbf{r})$ (j=A,B). After some manipulations we obtain

$$\mathcal{Z} = \int \mathscr{D}\phi_{\rm A}\mathscr{D}\omega_{\rm A}\mathscr{D}\phi_{\rm B}\mathscr{D}\omega_{\rm B} \exp\{-n\beta f_c[\phi_{\rm A},\phi_{\rm B},\omega_{\rm A},\omega_{\rm B}]\}$$

with

$$\begin{aligned}\beta f_c =& \frac{\chi N}{V}\int \mathrm{d}\mathbf{r}\mathrm{d}\mathbf{r}'\phi_{\rm A}(\mathbf{r})\beta u_0(|\mathbf{r}-\mathbf{r}'|)\phi_{\rm B}(\mathbf{r}') \\ &+\frac{N}{2\kappa V}\int \mathrm{d}\mathbf{r}\mathrm{d}\mathbf{r}'\left[\phi_{\rm A}(\mathbf{r})+\phi_{\rm B}(\mathbf{r})\right]\beta u_0(|\mathbf{r}-\mathbf{r}'|)\left[\phi_{\rm A}(\mathbf{r}')+\phi_{\rm B}(\mathbf{r}')\right] \\ &-\frac{1}{V}\int \mathrm{d}\mathbf{r}\left[\omega_{\rm A}(\mathbf{r})\phi_{\rm A}(\mathbf{r})+\omega_{\rm B}(\mathbf{r})\phi_{\rm B}(\mathbf{r})\right]-\ln Q[\omega_{\rm A},\omega_{\rm B}] \end{aligned} \tag{24}$$

where again the Stirling approximation is used, a constant factor is omitted in $\mathcal{Z}$, and the single-chain partition function is defined as $Q \equiv \prod_{s=1}^{N}\sum_{\mathbf{R}_s}\cdot\exp\left[-\sum_{s=1}^{N-1}\beta u_s^b-\sum_{s=1}^{N_{\rm A}}\omega_{\rm A}(\mathbf{R}_s)/N-\sum_{s=N_{\rm A}+1}^{N}\omega_{\rm B}(\mathbf{R}_s)/N\right]\Big/G$ with $G \equiv \prod_{s=1}^{N}\sum_{\mathbf{R}_s}\cdot\exp\left(-\sum_{s=1}^{N-1}\beta u_s^b\right) = V\left(4\pi\sqrt{\pi/6}/3(N-1)^{3/2}\right)^{N-1}$. This field theory is the starting point for analysis using the random-phase approximation,[33] which closely follows the Appendix 3 and 4 of our previous work[7] and gives the mean-field order-disorder transition of symmetric DBC, and derivation of the SCF equations given below.

The SCF equations are obtained from Eq. (24) by setting $\delta\beta f_c/\delta\phi_j(\mathbf{r}) = \delta\beta f_c/\delta\omega_j(\mathbf{r}) = 0$,

and can be written as

$$\hat{\omega}_{\mathrm{A}}(\mathbf{k}) = \beta\hat{u}_0(k)\left[\frac{N}{\kappa}\hat{\phi}_{\mathrm{A}}(\mathbf{k}) + \left(\frac{N}{\kappa} + \chi N\right)\hat{\phi}_{\mathrm{B}}(\mathbf{k})\right] \tag{25}$$

$$\hat{\omega}_{\mathrm{B}}(\mathbf{k}) = \beta\hat{u}_0(k)\left[\frac{N}{\kappa}\hat{\phi}_{\mathrm{B}}(\mathbf{k}) + \left(\frac{N}{\kappa} + \chi N\right)\hat{\phi}_{\mathrm{A}}(\mathbf{k})\right] \tag{26}$$

$$\phi_{\mathrm{A}}(\mathbf{r}) = \frac{\exp[\omega_{\mathrm{A}}(\mathbf{r})/N]}{N\hat{q}_N(\mathbf{k}=\mathbf{0})/V}\sum_{s=1}^{N_{\mathrm{A}}} q_s(\mathbf{r})q^*_{N-s+1}(\mathbf{r}) \tag{27}$$

$$\phi_{\mathrm{B}}(\mathbf{r}) = \frac{\exp[\omega_{\mathrm{B}}(\mathbf{r})/N]}{N\hat{q}_N(\mathbf{k}=\mathbf{0})/V}\sum_{s=N_{\mathrm{A}}+1}^{N} q_s(\mathbf{r})q^*_{N-s+1}(\mathbf{r}) \tag{28}$$

where we denote the Fourier transform of $\omega_j(\mathbf{r})$, for example, by $\hat{\omega}_j(\mathbf{k}) \equiv \int \mathrm{d}\mathbf{r} e^{-i\mathbf{k}\cdot\mathbf{r}}\omega_j(\mathbf{r})$ with $\mathbf{k}$ being the wave-vector, and $k \equiv |\mathbf{k}|$. The chain propagator $q_s(\mathbf{r})$ corresponds to the probability of finding a partial copolymer chain of s segments that starts from the A-end (where $s = 1$) anywhere in the system and ends at $\mathbf{r}$, and it satisfies the Chapman-Kolmogorov equation (CKE)[25]

$$q_{s+1}(\mathbf{r}) = \begin{cases} \exp[-\omega_{\mathrm{A}}(\mathbf{r})/N]\int \mathrm{d}\mathbf{r}'\Phi(|\mathbf{r}-\mathbf{r}'|)q_s(\mathbf{r}') & \text{for } s = 1,\ldots,N_{\mathrm{A}}-1 \\ \exp[-\omega_{\mathrm{B}}(\mathbf{r})/N]\int \mathrm{d}\mathbf{r}'\Phi(|\mathbf{r}-\mathbf{r}'|)q_s(\mathbf{r}') & \text{for } s = N_{\mathrm{A}},\ldots,N-1 \end{cases} \tag{29}$$

with the initial condition $q_1(\mathbf{r}) = \exp[-\omega_{\mathrm{A}}(\mathbf{r})/N]$, where $\Phi(r) = [3(N-1)/2\pi]^{d/2}\exp\left[-3(N-1)r^2/2\right]$ (note that chains propagate in 3D regardless of d). Similarly, the propagator $q^*_t(\mathbf{r})$ corresponds to the probability of finding a partial copolymer chain of t segments that starts from the B-end (where $t \equiv N - s + 1 = 1$) anywhere in the system

and ends at $\mathbf{r}$, and it satisfies the following CKE

$$q^*_{t+1}(\mathbf{r}) = \begin{cases} \exp[-\omega_{\rm B}(\mathbf{r})/N] \int {\rm d}\mathbf{r}' \Phi(|\mathbf{r}-\mathbf{r}'|) q^*_t(\mathbf{r}') & \text{for } t = 1, \ldots, N_{\rm B}-1 \\ \exp[-\omega_{\rm A}(\mathbf{r})/N] \int {\rm d}\mathbf{r}' \Phi(|\mathbf{r}-\mathbf{r}'|) q^*_t(\mathbf{r}') & \text{for } t = N_{\rm B}, \ldots, N-1 \end{cases} \tag{30}$$

with the initial condition $q^*_1(\mathbf{r}) = \exp[-\omega_{\rm B}(\mathbf{r})/N]$. Once the SCF equations are solved, the mean-field free energy per chain can be calculated as

$$\begin{aligned} \beta f_c = -\frac{1}{V} \int \frac{{\rm d}\mathbf{k}}{(2\pi)^3} \Big\{ \frac{N}{2\kappa} \left[\hat{\phi}_{\rm A}(\mathbf{k}) + \hat{\phi}_{\rm B}(\mathbf{k}) \right] \beta \hat{u}_0(k) \left[\hat{\phi}_{\rm A}(-\mathbf{k}) + \hat{\phi}_{\rm B}(-\mathbf{k}) \right] \\ + \chi N \hat{\phi}_{\rm A}(\mathbf{k}) \beta \hat{u}_0(k) \hat{\phi}_{\rm B}(-\mathbf{k}) \Big\} - \ln \frac{\hat{q}_N(\mathbf{k}=\mathbf{0})}{V}. \end{aligned} \tag{31}$$

The SCF equations are solved in real space with the periodic boundary conditions applied in all directions. The convolutions in Eqs. (29) and (30) are evaluated via the fast Fourier transforms,[34] and Eqs. (25) and (26) are solved via either the Broyden method combined with a globally convergent strategy[35] in 1D or the Anderson mixing[36] in 2D and 3D with an error $\varepsilon = \max[\text{abs}(\triangle\omega_A, \triangle\omega_B)] \leq 10^{-12}$. Our spatial discretization gives an accuracy of at least 10^{-5} in the calculated βf_c. We have only considered four ordered morphologies in this work: lamellae (L) in 1D, hexagonally packed cylinders (C) in 2D, and spheres arranged on a body-centered cubic lattice (S) and the double-gyroid (G) in 3D. For each of these morphologies, βf_c is minimized with respect to the calculation cell size to obtain its bulk period L_0 at given χN. These minimized βf_c, along with that of the disordered phase (D), are then used to determine the phase boundaries at given f.

In the limit of $N \to \infty$ at finite $R_{e,0}$, DGC becomes the continuous Gaussian chain

(CGC) model commonly used in polymer field theories. In addition, with $\sigma = 0$ and $\kappa = 0$, our model recovers the "standard" one (i.e., incompressible DBC melts of CGC interacting with the Dirac δ-function potential) used in polymer field theories, for which the SCF equations can be found in, for example, Ref. [37]. Incompressible melts corresponds to $N/\kappa \to \infty$.

There are several differences between DPD simulations and SCFT calculations. First, while DPD simulations include fluctuations and correlations, such effects are neglected by the mean-field approximation in SCF calculations. Second, DPD is a dynamic simulation technique while SCF is an equilibrium approach, which means that the morphology in DPD simulations could be kinetically trapped. Third, Groot and Madden[2] used a fixed-size box with periodic boundary conditions, which limit the allowed periods of the ordered structures, while SCF calculations can find the bulk period that minimizes the system free energy. Finally, DPD simulations have to be done for finite-size systems, while SCF calculations correspond to the thermodynamic limit. Thus comparisons between DPD simulations using DGC with the DPD potentials and the standard SCFT model for DBCs, as made by Groot and Madden, mix all these differences together.

In the results, comparisons of MC simulations SCF calculations using the same model are presented to unambiguously reveal the fluctuation and correlation effects. Furthermore, the SCF results of the standard model are compared with the DPD model to unambiguously reveal the model differences.

3 RESULTS AND DISCUSSION

For the DPD model system, unless specified otherwise, we use the same parameter values as in the DPD simulations,[2,3] i.e., $N = 10$, $\sigma/R_{e,0} = 2/3\sqrt{3}$, $N/\kappa = 50\pi$, $\chi N = 30\pi$ (at $\rho_0\sigma^3 = 3$) and 20π (at $\rho_0\sigma^3 = 5$).

3.1 SCF CASES AND ACCURACY

Table 1 shows the upper and lower limits of χN values, spatial discretization size, and free energy accuracy for our SCF calculations for different volume fractions and phases. For the 1D, 2D, and 3D phases our spatial discretization of 256, 128, and 96 respectively gives an accuracy of at least 10^{-5} in the calculated βf_c. For the upper limit of χN values for the different cases, the corresponding period l_0 is also shown.

Table 1: The upper and lower limits of χN values, spatial discretization size m, and free energy accuracy for our SCF calculations for different volume fractions and phases.

	Phase	χN_{min}	χN_{max}	$l_0(\chi N_{max})$	m	βf_c accuracy
	L	63.300	95.000	2.538	256	4.31×10^{-07}
f=0.1	C	50.100	82.000	1.988	128×224	8.96×10^{-06}
	S	47.700	80.000	2.212	96	3.39×10^{-05}
	L	25.509	95.000	2.633	256	
f=0.2	C	22.767	47.500	2.121	128×224	4.40×10^{-06}
	S	21.991	52.000	2.607	96	2.67×10^{-06}
	L	15.713	95.000	2.645	256	
f=0.3	C	15.119	45.000	2.380	128×224	
	S	14.911	50.000	3.044	96	
	L	12.318	95.000	2.657	256	
f=0.4	C	12.216	19.000	2.061	128×224	1.24×10^{-07}
	S	12.196	17.000	2.450	96	
	G	12.300	16.770	4.228	96	8.78×10^{-06}
f=0.5	L	11.427	95.000	2.662	256	

The phase boundaries for the multiple cases were calculated by fitting a third-order polynomial to the free energy curves and determining the value of χN where the free energies are equal. The spatial accuracy in βf_c was determined by running simulations for constant parameters and varying the spatial discretization, m. Fig 1 shows the accuracy relative to $m = 2048$ for varying spatial discretization for the symmetric DBC ($f = 0.5$) case. At $m = 2048$, the difference in free energy is on the order of the floating-point accuracy of computers.

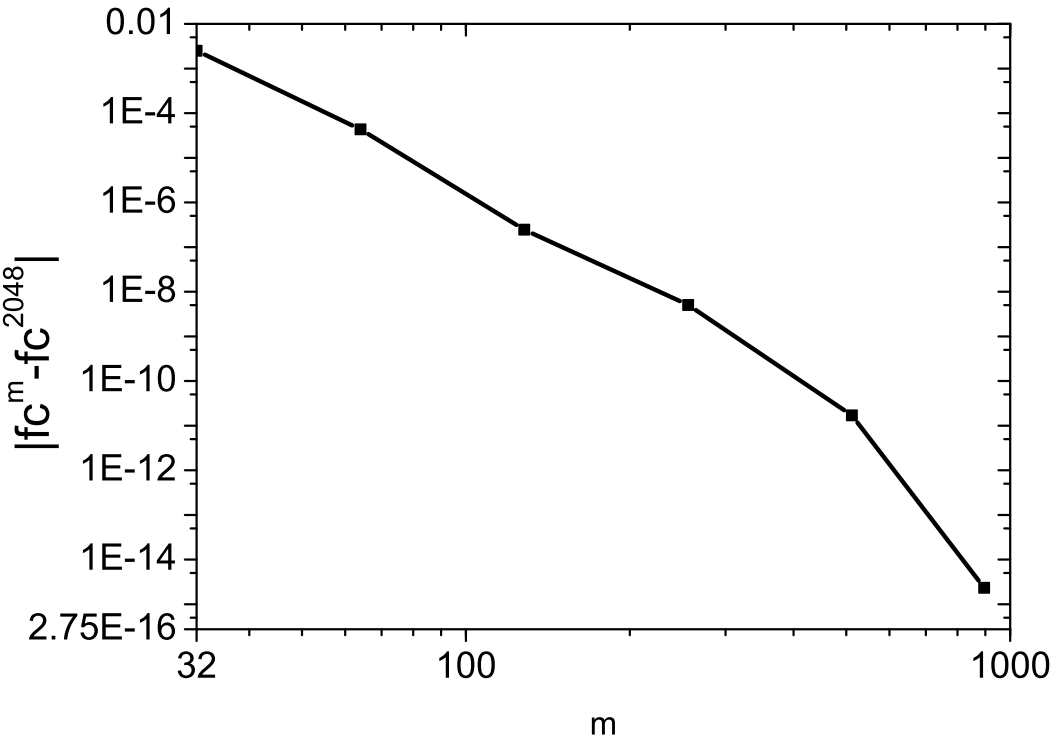

Figure 1: Spatial accuracy in βf_c relative to $m = 2048$ for symmetric DBC ($f = 0.5$). At $m = 2048$, the difference in free energy is on the order of the floating-point accuracy of computers.

3.2 SYMMETRIC DBC

3.2.1 ORDER-DISORDER TRANSITION (ODT)

For the results, we will first look at the order-disorder transition (ODT) of symmetric DBCs ($f = 0.5$). Table 2 shows the mean-field ODT for various combinations of either continuous Gaussian chains (CGC) or discrete Gaussian chains (DGC) with either the Dirac δ-function repulsion or the DPD potential, βu_0, thus highlighting the effects of chain discretization and interaction range. With increasing interaction range σ, both the mean-field ODT $\chi^*_{MF}N$ and the lamellar period $L^*_{0,MF}/R_{e,0}$ in parenthesis increase. This is consistent with previous work done by Wang.[38] Since A-B repulsion becomes larger due to an increase in interaction range of $u^{\chi}(r)$, an increase in l_0 results to restore the balance between the A-B repulsion and chain stretching.[38] The increase in χ^*N observed in experiments from the mean-field result is not entirely due to fluctuations since small but finite interaction range is present in real systems.[38] With decreasing chain discretization N, however, $\chi^*_{MF}N$ decreases and $L^*_{0,MF}/R_{e,0}$ increases.

Table 2: Mean-field ODT $\chi^*_{\mathrm{MF}}N$ and the corresponding bulk lamellar period $L^*_{0,\mathrm{MF}}$ of symmetric DBC for four combinations of chain model with non-bonded interaction potential, obtained from RPA. The upper-left corresponds to the "standard" model and the lower-right to the DPD model system.

$\chi^*_{\mathrm{MF}}N(L^*_{0,\mathrm{MF}}/R_{e,0})$	δ-function potential	DPD-potential
CGC	10.495 (1.318)	12.134 (1.462)
DGC with $N = 10$	9.944 (1.345)	11.427 (1.495)

Looking at the standard model (CGC, δ) and the DPD model (DGC, βu_0) in Table 2, we notice that the mean-field ODT is not affected by the system compressibility. Based

on previous work done by Wang,[38] it was shown that although the increase in system compressibility (i.e, decreasing N/κ) decreases both f_c and l_0, it has no effect on the mean-field ODT. As the compressibility is increased (i.e., i N/κ), l_0 decreases to account for the reduction in A-B repulsion resulting from stronger segregation of the A and B segments. Similarly, as the system becomes incompressible ($N/\kappa \to \infty$), the segments become hardspheres resulting in an increase in l_0. We note in Fig. 2 the phase transition from the disordered phase to the lamella phase is a second-order phase transition, and it was shown by Wang[38] that a finite compressibility still results in a second-order phase transition.[EXPLAIN-need Matsen's email for explanation on 2nd-order phase transition]

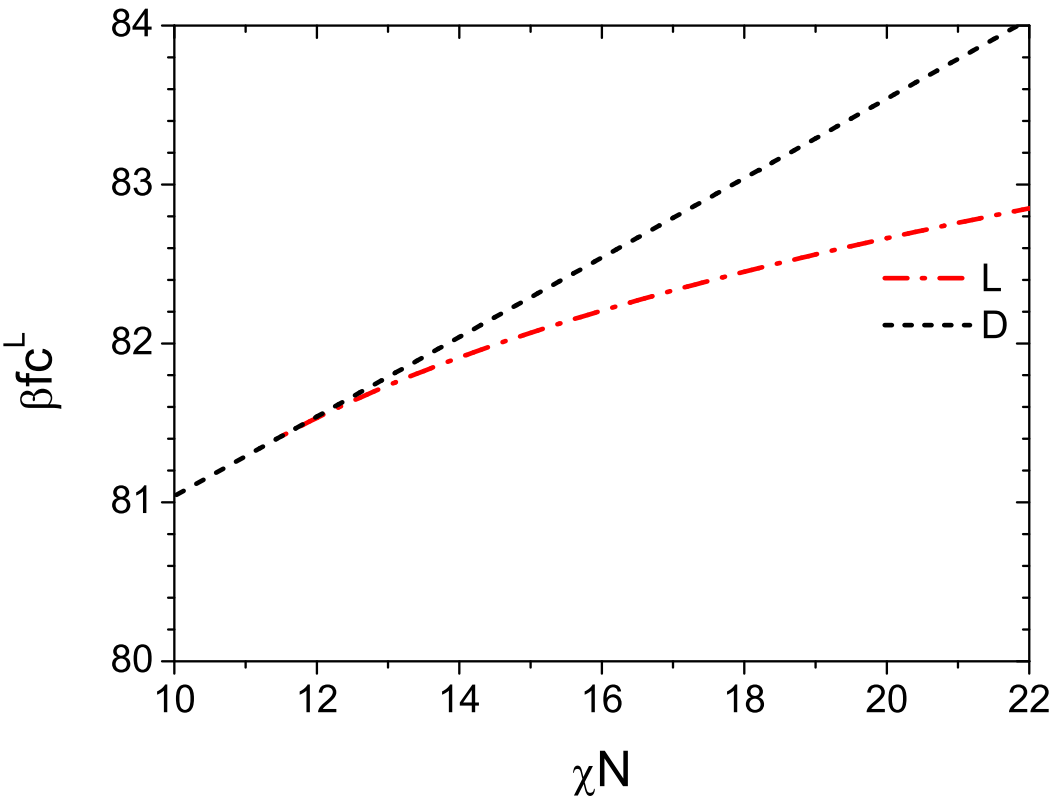

Figure 2: Second-order phase transition for symmetric DBC ($f = 0.5$) from lamella to disordered shown by comparing the free energy of the lamella βf_c^L (L) in comparison to the free energy of the disordered phase (D).

Fig. 3 shows the lamellar period as a function of χN. Note that the period monotonically increases with χ.

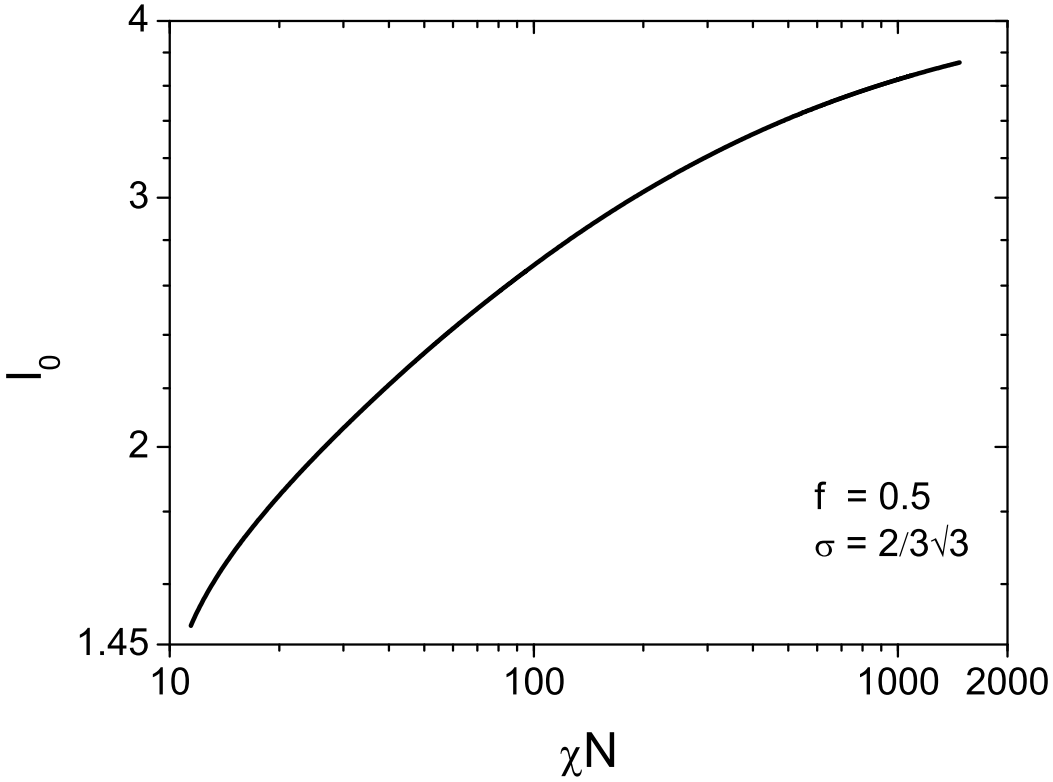

Figure 3: The lamellar period l_0 as a function of χN.

Table 3 shows the ODT $\chi^* N$ and the corresponding bulk lamellar period L_0^* determined from our FOMC simulations of the DPD model system. We see that both $\chi^* N$ and L_0^* are significantly larger than the corresponding mean-field value due to the large system fluctuations/correlations, which are expected for the small $\bar{\mathcal{N}}$-values used in the simulations. Another well-known effect of fluctuations on ODT of symmetric DBC is to change it from a second-order phase transition predicted by the mean-field theory to a first-order transition.[17,26]

To compare their DPD simulations with the SCF results for the "standard" model, Groot and Madden mapped the interaction parameters $a_{\rm AA} = a_{\rm BB}$ and $a_{\rm AB}$ in the simulations to the Flory-Huggins χ parameter in the "standard" model (denoted by χ_e hereafter) using the following relation valid for $\chi_e > 3$:

$$\chi_e = \begin{cases} (0.306 \pm 0.003)(a_{\rm AB} - a_{\rm AA}) & \text{for } \rho_0\sigma^3 = 3 \text{ and } 2 < N < 10 \\ (0.689 \pm 0.002)(a_{\rm AB} - a_{\rm AA}) & \text{for } \rho_0\sigma^3 = 5 \text{ and } N = 1 \end{cases} . \qquad (32)$$

This relation was obtained by Groot and Warren via fitting the domain segregation from canonical-ensemble DPD simulations of phase-separated symmetric mixtures of A and B monomers (at $\rho_0\sigma^3 = 5$) and homopolymers (at $\rho_0\sigma^3 = 3$, where a value of 2 instead of 4 was used in the spring force given in Eq. (8)) to the corresponding prediction of the Flory-Huggins theory,[23] and its use by Groot and Madden clearly has no rigorous basis.

To account for the fluctuation effects neglected by the SCF calculations, Groot and Madden further used an "effective" χ-parameter $\chi_{e,f} = \chi_e/(1 + 3.91\bar{\mathcal{N}}^{-1/3})$ based on FH theory,[17] which gives $\chi^*/\chi^*_{\rm MF} - 1 = 3.91\bar{\mathcal{N}}^{-1/3}$. The values of $\chi_e N$ and $\chi_{e,f} N$ corresponding to $\chi^* N$ determined from our FOMC simulations are also listed in Table 3; at both densities, $\chi_{e,f} N$ is clearly different from the mean-field ODT for the "standard" model (i.e., 10.495). As explained in Introduction, the small $\bar{\mathcal{N}}$-values in the DPD simulations do not justify the use of FH theory which is rigorously accurate only for $\bar{\mathcal{N}} \geq 10^{10}$; our FOMC data in Table 3 give $\chi^*/\chi^*_{\rm MF} - 1 = 31.16\bar{\mathcal{N}}^{-0.63}$ if the power-law is assumed. Finally, we note that another way to calculate $\chi_{e,f}$ used in Ref. [2] (see Eq. (13) there), which gives "a near quantitative

match with the mean-field theory" as claimed by Groot and Madden,[2] results in $\chi_{e,f}N \approx 16$ at both densities.

Table 3: ODT χ^*N and the corresponding bulk lamellar period L_0^* of symmetric DBC for the DPD model at given segmental number density $\rho_0\sigma^3$, obtained from FOMC simulations. The corresponding values of the invariant degree of polymerization $\bar{\mathcal{N}}$, the Flory-Huggins parameter χ_e, and that corrected for the fluctuation effects based on FH theory $\chi_{e,f}$ are also listed. See main text for more details.

$\rho_0\sigma^3$	$\bar{\mathcal{N}}$	χ^*N	χ_e^*N	$\chi_{e,f}^*N$	$L_0^*/R_{e,0}$
3	≈ 28	55.08 ± 0.47	26.82 ± 0.82	11.70 ± 0.36	2.203 ± 0.001
5	≈ 77	34.31 ± 0.82	22.57 ± 0.57	11.76 ± 0.30	2.053 ± 0.003

3.2.2 FLUCTUATION/CORRELATION EFFECTS ON LAMELLAE

Next, we examine the fluctuation/correlation effects on strongly segregated lamellae. Table 4 shows under the condition that $\rho_0\sigma^3 = 3(\bar{\mathcal{N}} \approx 28, \chi N = 30\pi)$ for the DPD model, our Monte Carlo simulations give a smaller bulk period than predicted by the self-consistent field theory, while Groot and Madden[2] used a larger period.

Table 4: Bulk period obtained from MC, SCF and DPD.

$\rho_0\sigma^3 = 3(\bar{\mathcal{N}} \approx 28, \chi N = 30\pi)$	
	$L_0/R_{e,0}$
MC	2.50± 0.01
SCF	2.658
DPD[2]	2.722

Fig. 4 compares the relative fraction of A segments within the lamellae obtained from our

MC simulations and SCF calculations; we see that the simulations give a much larger A-B interfacial width, due to the capillary-wave fluctuations of the interfaces that are neglected by the SCF calculations. Fig. 5 compares the total polymer density profile in the lamellae. Since

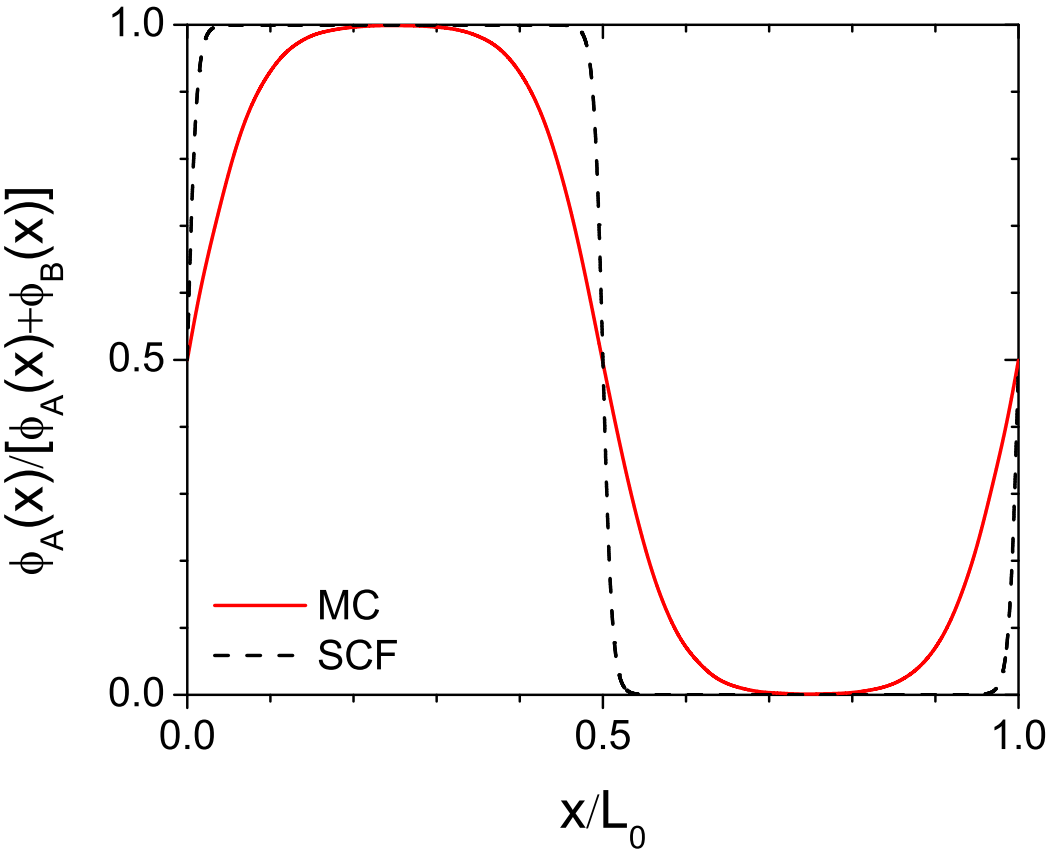

Figure 4: Comparisons of the ensemble-averaged profiles of the relative fraction of A segments in the direction (denoted by x) perpendicular to the lamellar interfaces, $\tilde{\phi}_{\rm A}(x) \equiv \langle \phi_{\rm A}(x)/[\phi_{\rm A}(x)+\phi_{\rm B}(x)] \rangle$ obtained from our SCF calculations and FOMC simulations of the DPD model at $\chi N = 30\pi$ ($\bar{\mathcal{N}} \approx 28$ in the simulations), where the bulk lamellar period $L_0/R_{e,0} = 2.658$ in the SCF calculations and 2.50 ± 0.01 in the FOMC simulations.

the DPD model is compressible, we see large density oscillations near the A-B interfaces in SCF calculations, which are strongly suppressed in MC simulations again due to the system fluctuations.

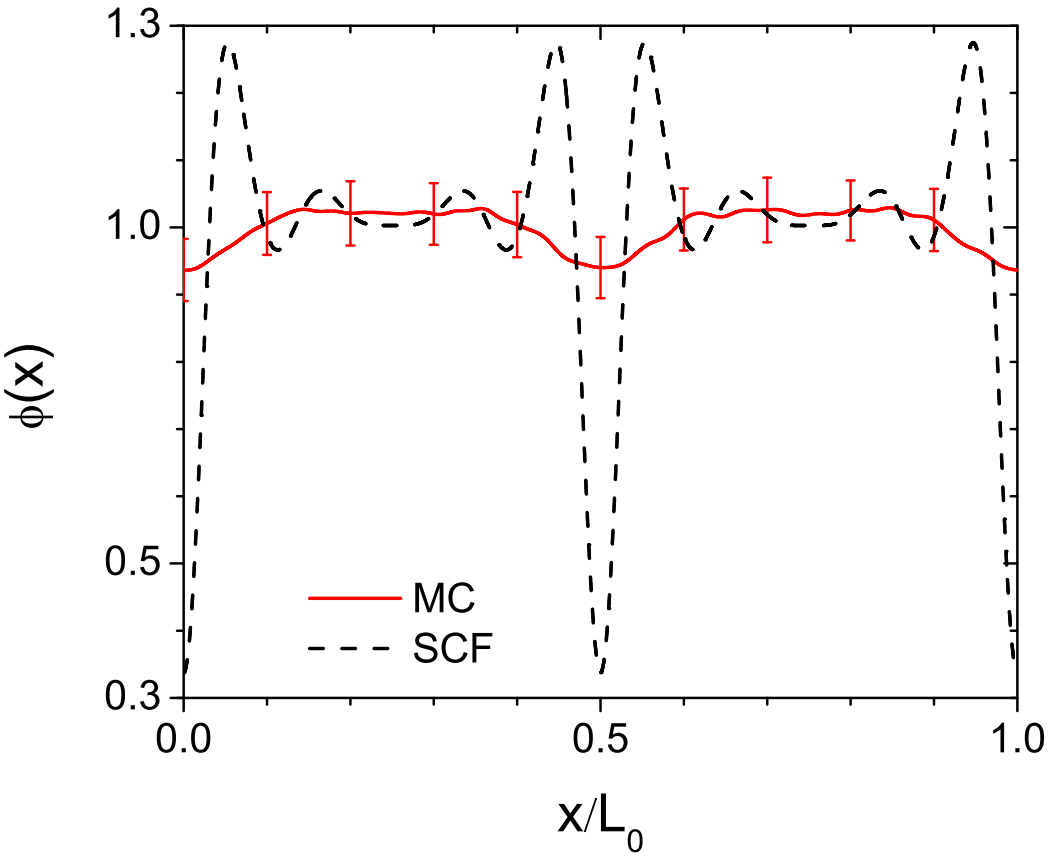

Figure 5: Comparisons of the ensemble-averaged profiles of the total segmental density in the x-direction, $\phi(x) \equiv \langle \phi_{\rm A}(x) + \phi_{\rm B}(x) \rangle$ obtained from our SCF calculations and FOMC simulations of the DPD model at $\chi N = 30\pi$ ($\bar{\mathcal{N}} \approx 28$ in the simulations), where the bulk lamellar period $L_0/R_{e,0} = 2.658$ in the SCF calculations and 2.50 ± 0.01 in the FOMC simulations.

3.3 ASYMMETRIC DBC SCF RESULTS

For asymmetric DBC at A-block volume fraction of $f = 0.4$, Fig. 6 shows the free energy per chain βf_c of various ordered phases relative to that of the disordered phase obtained from SCF calculations. We see that, with increasing χN, the stable phase having the lowest βf_c changes in the sequence of D→S→C→G→L; the stable regions of the order phases are listed in Table 5. Note that we haven't included hexagonally closely packed spheres and the complicated Fddd phase in our calculations. This sequence is the same as found for the "standard" model, but all the phase boundaries are shifted to higher χN compared to the latter, as also shown in Table 5. We attribute this to the finite interaction range $\sigma > 0$ in the DPD model, which is consistent with our RPA results on the mean-field ODT of symmetric DBC shown in Table 2. That $\sigma > 0$ shifts the phase boundaries to higher χN is also found by Matsen in his recent SCF calculations of incompressible DBC melts modeled as freely jointed chains with a Gaussian non-bonded repulsive potential between A and B segments.[38]

Fig. 7 compares βf_c of various phases obtained from our SCF calculations of the DPD model at $f = 0.3$, where L is unstable. In addition, we have not been able to find G at all, suggesting that it also be unstable. With increasing χN, the stable phase now changes in the sequence of D→S→C. As in the $f = 0.4$ case above, this sequence is the same as found for the "standard" model with all the phase boundaries shifted to higher χN as shown in Table 5. The same is found at $f = 0.2$ in Fig. 8, as also shown in Table 5.

Finally, at $f = 0.1$, our SCF results shown in Fig. 9 and Table 5 indicate that S is the only

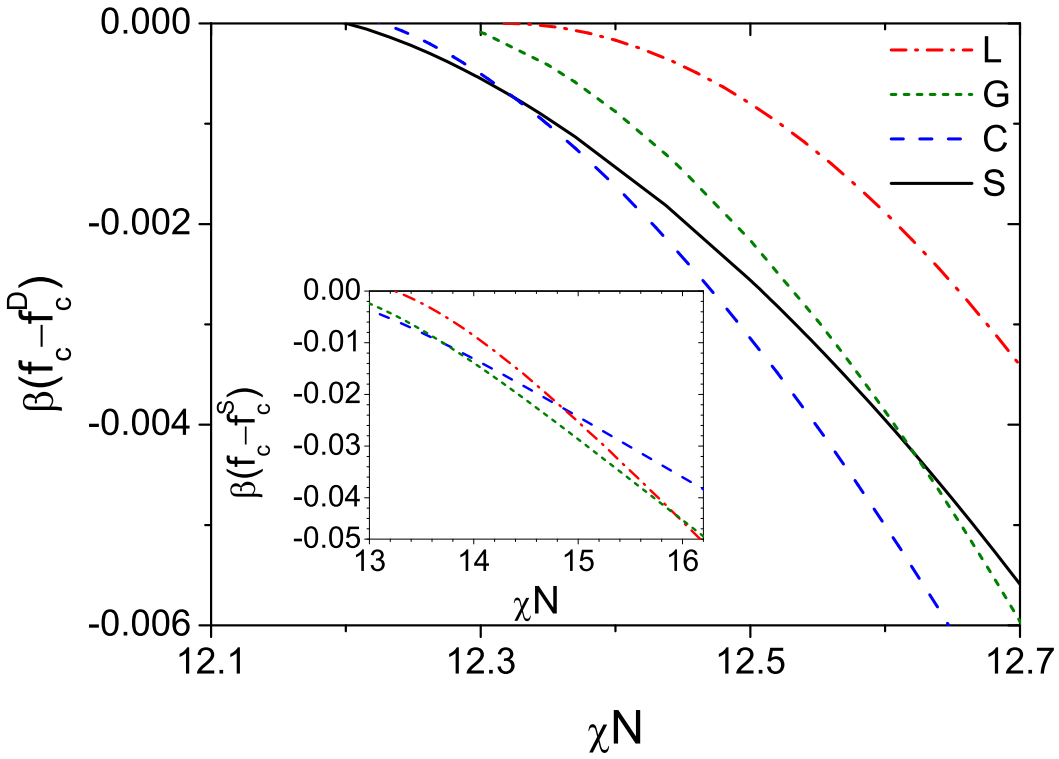

Figure 6: Free energy per chain βf_c of various ordered phases relative to the disordered phase obtained from SCF calculations for asymmetric DBCs for $f = 0.4$. The sub plot shows βf_c of various ordered phases relative to the free energy per chain of the spheres βf_c^S at higher χN.

stable ordered phase, again consistent with the "standard" model. Different from the above cases, however, χN at the D/S transition is lower than that for the "standard" model. We attribute this to the finite chain discretization $N = 10$ in the DPD model (i.e., only one segment in the A-block), which is consistent with our RPA results on the mean-field ODT of symmetric DBC shown in Table 2.

Table 5

Stable regions in χN of various ordered phases obtained from the SCF calculations of the DPD and the "standard" models; results for the latter model are provided by Mark Matsen. For each A-block volume fraction in the copolymer f, the stable phase (having the lowest Helmholtz free energy per chain) is replaced by that in a lower row at higher χN. The last column lists the χN-values at which the DPD simulations[2,3] were performed; the morphology obtained from the DPD simulations is given in parentheses if it is different from the SCF prediction. See main text for more details.

f	Phase	SCF Results		Morphology Found in DPD Simulations
		DPD model	"standard" model	
0.5	L	>11.427	>10.495	20π, 30π
0.4	S	>12.215	>11.231	
	C	>12.324	>11.373	
	G	>13.730	>12.786	
	L	>15.933	>15.352	20.5 ± 0.2 (D)[a], 41.1 ± 0.4 ("liquid rods"), 61.6 ± 0.6 ("random network"), 82.1 ± 0.8 ("like gyroid"), 30π, 102.7 ± 1.0, 123.2 ± 1.2
0.3	S	>15.007	>13.917	
	C	>15.970	>14.989	20π, 30π
0.2	S	>22.373	>21.136	
	C	>28.589	>27.740	41.1 ± 0.4 (D), 61.6 ± 0.6 ("micellar"), 20π ("micellar"), 82.1 ± 0.8 ("micellar"), 30π ("micellar"), 102.7 ± 1.0 ("long micellar"), 123.2 ± 1.2
0.1	S	>47.181	>47.956	30π (D)

[a] Also found at $f = 0.2$.

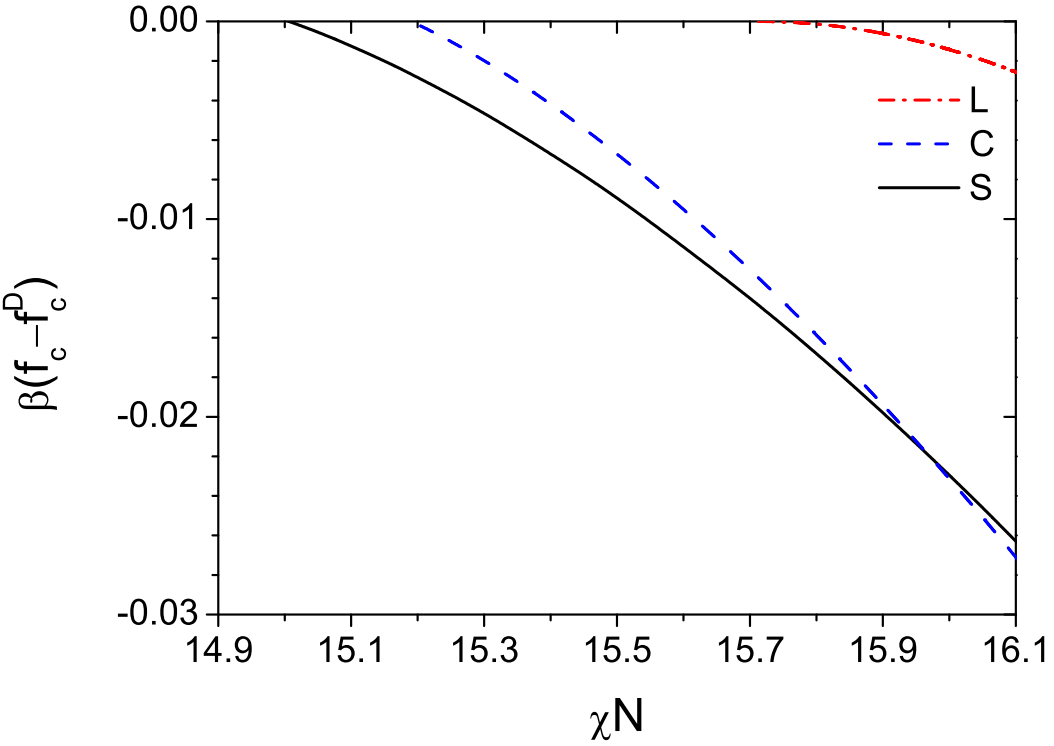

Figure 7: Free energy per chain βf_c of various phases relative to the disordered phase obtained from our SCF calculations of the DPD model at $f = 0.3$

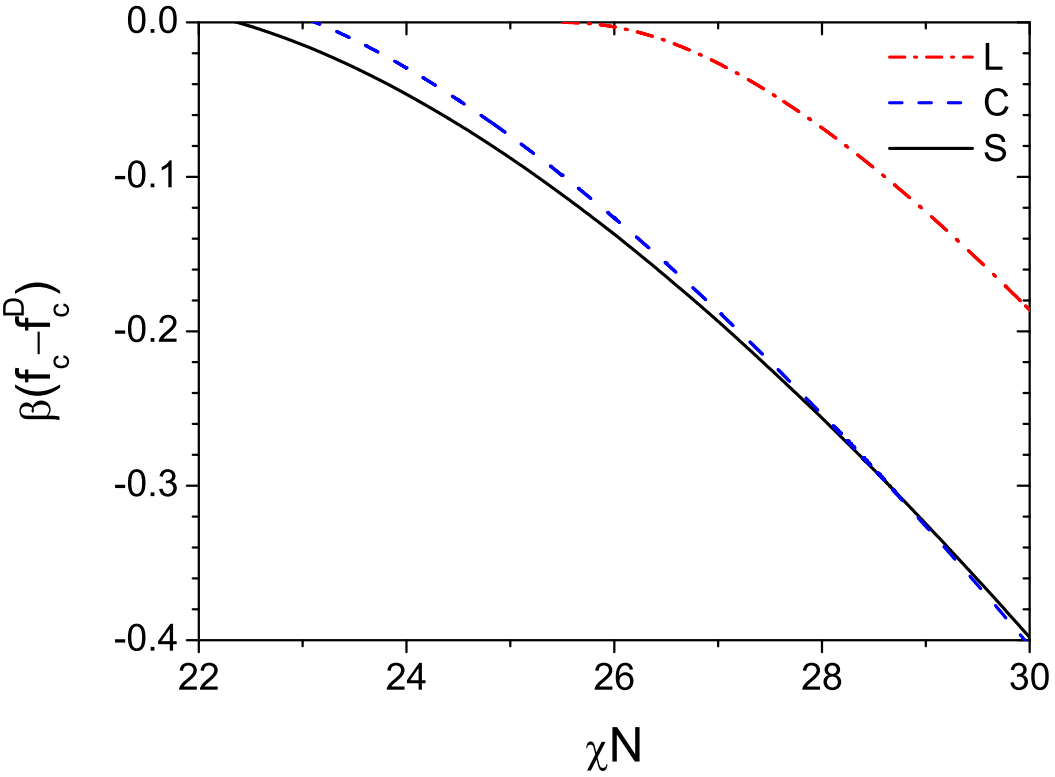

Figure 8: Free energy per chain βf_c of various phases relative to the disordered phase obtained from our SCF calculations of the DPD model at $f = 0.2$

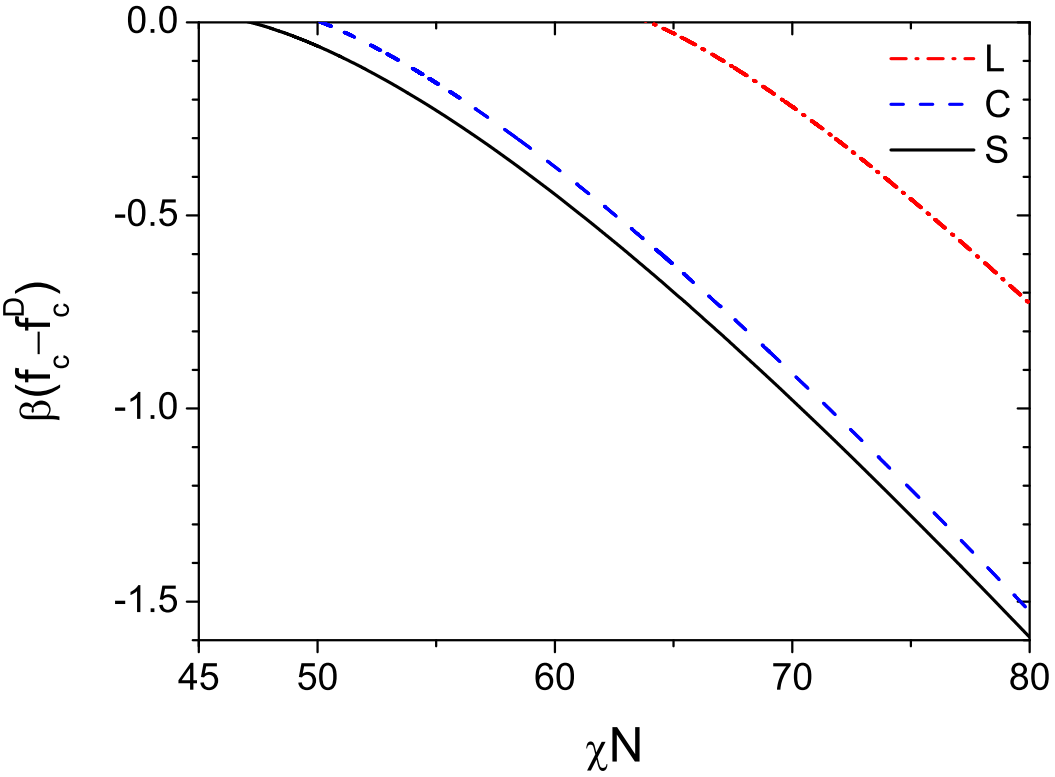

Figure 9: Free energy per chain βf_c of various phases relative to the disordered phase obtained from our SCF calculations of the DPD model at $f = 0.1$

3.4 COMPARING MORPHOLOGIES IN SCF CALCULATIONS AND DPD SIMULATIONS

Using a cubic box of $(20\sigma)^3$, Groot and Madden performed DPD simulations at $\chi N = 30\pi$ (with $\rho_0\sigma^3 = 3$) and 20π (with $\rho_0\sigma^3 = 5$),[2] and Chen et al. performed DPD simulations at more χN-values (with $\rho_0\sigma^3 = 3$).[3] Table 5 also lists the morphologies obtained in these DPD simulations; as the values of $\chi_e N$ instead of a_{ij} were reported in Ref. [3], their χN-values have a small error bar due to the use of Eq. (32). In eleven of the totally 20 cases (f-χN combinations) studied, a morphology different from that predicted by the SCF calculations was obtained, mostly at $f = 0.4$ and 0.2. We focus on these discrepancies in the following.

As shown in Table 3, our FOMC simulations give $\chi^* N = 55.08 \pm 0.47$ for symmetric DBC with $\rho_0\sigma^3 = 3$; for asymmetric DBC, we expect the ODT to be at higher χN, which means that the disordered phase found in the DPD simulations at $f = 0.4$ ($\chi N = 20.5 \pm 0.2$) and 0.2 ($\chi N = 41.1 \pm 0.4$)[3] is due to the large system fluctuations neglected in the SCF calculations. In the case of $f = 0.1$ ($\chi N = 30\pi$), where the ODT is unknown, mismatch between the cubic simulation box and the bulk period of S could also lead to the disordered phase found in the DPD simulations.[2] On the other hand, the "liquid rods" morphology found in the DPD simulations at $f = 0.4$ ($\chi N = 41.1 \pm 0.4$)[3] is questionable, as their χN-value is even below our ODT for symmetric DBC.

The "random network" and "like gyroid" morphologies found in the DPD simula-

tions at $f = 0.4$ ($\chi N = 61.6 \pm 0.6$ and 82.1 ± 0.8, respectively)[3] are interesting and may correspond to G in the SCF calculations. Mismatch between the cubic simulation box and the bulk period of G, however, needs to be considered, which strongly affects the observation of G in fixed-box simulations.[39]

Finally, the "micellar" and "long micellar" morphologies found in most DPD simulations at $f = 0.2$[2,3] may be due to the mismatch between the cubic simulation box and the bulk period of C. As DPD is a dynamic simulation technique, these poorly ordered morphologies could also be kinetically trapped.

4 SUMMARY

Using soft potentials such as that for the conservative force in the dissipative particle dynamics (DPD) simulations[1,4] is the basic idea of the so-called fast Monte Carlo (FMC) simulations,[7–9] which in principle give the same thermodynamic properties as the DPD simulations.[4] In this work, we revisit the comparisons made by Groot and Madden[2,18] and Chen et al.[3] between their DPD simulations of the DPD model (i.e., a compressible system of discrete Gaussian chains each of $N = 10$ segments interacting with a finite-range (DPD) potential) and the self-consistent field (SCF) calculations of the "standard" model[16] (i.e., an incompressible system of continuous Gaussian chains interacting with the Dirac δ-function potential) for diblock copolymer (DBC) A-B melts, where the model differences were mixed with the following differences between the two methods: (1) DPD simulations sample the full spectrum of fluctuations/correlations of the system, which are neglected in SCF calculations; (2) morphologies found in DPD simulations could be kinetically trapped, while SCF is an equilibrium approach; (3) the DPD simulations[2,3,18] are performed in a fixed-size box, which limits the allowed periods of the ordered structures,[21] while the SCF calculations[16] find the bulk period of all ordered phases; and (4) binary blends of DBC with different compositions (volume fractions of the A-block in the copolymer) f are used in most of the simulations by Groot and Madden,[2,18] while the SCF calculations[16] are for pure DBC systems.

We perform both SCF calculations and FMC simulations in a canonical ensemble based on the DPD model; note that our FMC simulations performed in variable-size boxes

can find the bulk period of lamellar and cylindrical structures. Comparing our SCF results with those for the "standard" model therefore unambiguously reveals the effects of model differences (i.e., the system compressibility, chain discretization N, and interaction range σ), and comparing our SCF and FMC results reveals, without any parameter-fitting, the effects of system fluctuations/correlations neglected in the SCF theory. Furthermore, comparing our FMC results with the DPD results obtained in the same fixed-size box unambiguously identifies the kinetically trapped structures in the latter, and comparing our SCF (or FMC) results in both fixed- and variable-size boxes unambiguously reveals the effects of fixed vs. bulk periods. For simplicity, we only consider systems of pure DBC and four ordered morphologies in this work: lamellae, hexagonally packed cylinders, spheres arranged on a body-centered cubic lattice, and the double-gyroid.

For symmetric DBC, the mean-field ODT $\chi^*_{\rm MF}N$ and the corresponding bulk lamellar period $L^*_{0,\rm MF}$ (as listed in Table 2) are not affected by the system compressibility N/κ[37] and the invariant degree of polymerization $\bar{\mathcal{N}}$, where χ and κ are the generalized Flory-Huggins interaction parameter and the generalized Helfand compressibility[24,25] defined in the DPD model (see Eq. (23)). Consistent with our previous work,[7,37] we find that $\chi^*_{\rm MF}N$ increases with both increasing σ and increasing N, and $L^*_{0,\rm MF}$ increases with increasing σ but decreasing N. On the other hand, the ODT χ^*N and the corresponding bulk lamellar period L^*_0 determined from our FOMC simulations of the DPD model (as listed in Table 3) are significantly larger than the corresponding mean-field value due to the large system fluctuations/correlations expected for the small $\bar{\mathcal{N}}$-values used in the simulations. Such small $\bar{\mathcal{N}}$-values do not justify the use of the fluctuation theory of Fredrickson and Helfand[17] by

Groot and Madden, and the parameter-fitting (i.e., the use of Eq. (32)) in their comparisons with the SCF results of the "standard" model also has no rigorous basis. Finally, consistent with our previous work,[40] for well-ordered lamellae we find that the capillary-wave fluctuations at the A-B interfaces increase the interfacial width, and that the system fluctuations greatly suppress the large depletion of the total segmental density at the A-B interfaces as well as its oscillations in lamellar domains predicted by our SCF calculations. Similar results are also found for well-ordered, hexagonally packed cylinders at $f = 0.3$ (and 0.7).

As summarized in Table 5, at all values of f (which are integer multiples of 0.1) our SCF calculations of the DPD model give the same sequence of phase transitions with varying χN as the "standard" model. All phase boundaries, however, are shifted to higher χN due to $\sigma > 0$, except at $f = 0.1$ (and 0.9), where χN at the transition between the disordered phase and the spheres arranged on a body-centered cubic lattice is lower due to $N = 10$ in the DPD model. Finally, Table 5 also compares, without any parameter-fitting, the morphologies obtained in the DPD simulations[2,3] with the SCF predictions. In eleven of the totally 20 cases (f-χN combinations) studied, a morphology different from the SCF prediction was obtained due to the aforementioned differences (1)$\sim$(3) between the two methods.

We emphasize that the goal of this work is not to invalidate the DPD model/method, but to highlight the importance of quantitative and parameter-fitting-free comparisons among different models/methods. In fact, with the numerical SCF calculations well-developed and widely applied to various polymeric systems,[22] it is of great interest to achieve quantitative understanding of the fluctuation/correlation effects neglected by the SCF calculations. For

this purpose, it is invaluable to develop particle-based models/methods such as DPD[1,4] or fast Monte Carlo simulations[7–9] and field-based models/methods such as the field-theoretic simulations.[41] Direct comparisons between these simulations and SCF calculations based on the same model system, thus without any parameter-fitting, can unambiguously quantify the fluctuation/correlation effects in the system.[12–14]

REFERENCES

[1] P. J. Hoogerbrugge and J. M. V. A. Koelman. "Simulating microscopic hydrodynamic phenomena with dissipative particle dynamics". *Europhys. Lett.*, **19**(3):155–160, 1992.

[2] R. D. Groot and T. J. Madden. "Dynamic simulation of diblock copolymer microphase separation". *J. Chem. Phys.*, **108**(20):8713–8724, 1998.

[3] L. J. Chen, Z. Y. Lu, H. J. Qian, Z. S. Li, and C. C. Sun. "The effects of Lowe-Andersen temperature controlling method on the polymer properties in mesoscopic simulations". *J. Chem. Phys.*, **122**(10), 2005.

[4] P. Espanol and P. Warren. "Statistical mechanics of dissipative particle dynamics". *Europhys. Lett.*, **30**(4):191–196, 1995.

[5] S. M. Willemsen, T. J. H. Vlugt, H. C. J. Hoefsloot, and B. Smit. "Combining dissipative particle dynamics and Monte Carlo techniques". *J. Comput. Phys.*, **147**(2):507–517, 1998.

[6] C. M. Wijmans, B. Smit, and R. D. Groot. "Phase behavior of monomeric mixtures and polymer solutions with soft interaction potentials". *J. Chem. Phys.*, **114**(17):7644–7654, 2001.

[7] Q. Wang and Y. H. Yin. "Fast off-lattice Monte Carlo simulations with "soft" repulsive potentials". *J. Chem. Phys.*, **130**(10):104903, 2009.

[8] Q. Wang. "Studying soft matter with "soft" potentials: Fast lattice Monte Carlo simulations and corresponding lattice self-consistent field calculations". *Soft Matter*, **5**(22):4564–4567, 2009.

[9] Q. Wang. "Correction – Studying soft matter with "soft" potentials: Fast lattice Monte Carlo simulations and corresponding lattice self-consistent field calculations". *Soft Matter*, **6**(24):6206–6207, 2010.

[10] F. A. Detcheverry, D. Q. Pike, P. F. Nealey, M. Muller, and J. J. de Pablo. "Monte Carlo simulation of coarse grain polymeric systems". *Phys. Rev. Lett.*, **102**(19):197801, 2009.

[11] D. Q. Pike, F. A. Detcheverry, M. Muller, and J. J. de Pablo. "Theoretically informed coarse grain simulations of polymeric systems". *J. Chem. Phys.*, **131**(8):084903, 2009.

[12] P. Zhang, X. Zhang, B. Li, and Q. Wang. "Quantitative study of fluctuation effects by fast lattice Monte Carlo simulations. I. Compressible homopolymer melts". *Soft Matter*, **7**(9):4461–4471, 2011.

[13] P. Zhang, B. Li, and Q. Wang. "Quantitative study of fluctuation effects by fast lattice Monte Carlo simulations. 2. Homopolymer brushes in an implicit, good solvent". *Macromolecules*, **44**(19):7837–7852, 2011.

[14] P. Zhang, B. Li, and Q. Wang. "Quantitative study of fluctuation effects by fast lattice Monte Carlo simulations. III. Homopolymer brushes in an explicit solvent". *Macromolecules*, **45**(5):2537–2550, 2012.

[15] J. Zong, X. Zhang, and Q. Wang. "Fast off-lattice Monte Carlo simulations of soft-core spherocylinders: Isotropic-nematic transition and comparisons with virial expansion". *J. Chem. Phys.*, **137**(13):134904, 2012.

[16] M. W. Matsen and F. S. Bates. "Unifying weak- and strong-segregation block copolymer theories". *Macromolecules*, **29**(4):1091–1098, 1996.

[17] G. H. Fredrickson and E. Helfand. "Fluctuation effects in the theory of microphase separation in block copolymers". *J. Chem. Phys.*, **87**(1):697–705, 1987.

[18] R. D. Groot and T. J. Madden. "Dissipative particle dynamics simulation of diblock copolymer microphase separation". In Lal, M. and Mashelkar, R. A. and Kulkarni, B. D. and Naik, V. M., editor, *Structure and dynamics of materials in the mesoscopic domain*, pages 288–301, 1999. 4th Meeting of the Royal-Society-Unilever-Indo-UK Forum in Materials Science and Engineering, NATL CHEM LAB, PUNE, INDIA, ,.

[19] S. A. Brazovskii. "Phase transition of an isotropic system to a nonuniform state". *Sov. Phys. JETP*, **41**(1):85–89, 1975.

[20] T. Ohta and K. Kawasaki. "Equilibrium morphology of block copolymer melts". *Macromolecules*, **19**(10):2621–2632, 1986.

[21] Q. Wang, Q. L. Yan, P. F. Nealey, and J. J. de Pablo. "Monte Carlo simulations of diblock copolymer thin films confined between two homogeneous surfaces". *J. Chem. Phys.*, **112**(1):450–464, 2000.

[22] G. H. Fredrickson. *The Equilibrium Theory of Inhomogeneous Polymers*. Oxford University Press, 2006.

[23] R. D. Groot and P. B. Warren. "Dissipative particle dynamics: Bridging the gap between atomistic and mesoscopic simulation". *J. Chem. Phys.*, **107**(11):4423–4435, 1997.

[24] E. Helfand and Y. Tagami. "Theory of interface between immiscible polymers". *J. Polym. Sci., Part B: Polym. Lett.*, **9**(10):741–746, 1971.

[25] E. Helfand and Y. Tagami. "Theory of interface between immiscible polymers. II". *J. Chem. Phys.*, **56**(7):3592–3601, 1972.

[26] J. Zong and Q. Wang. "Fluctuations/correlations in symmetric diblock copolymer melts. I. On the order-disorder transition". *Macromolecules*, **to be submitted**, 2012.

[27] S. D. Stellman and P. J. Gans. "Efficient computer simulation of polymer conformation. I. Geometric properties of hard-sphere model". *Macromolecules*, **5**(4):516–526, 1972.

[28] O. F. Olaj, B. Neubauer, and G. Zifferer. "Monte Carlo investigations of dense copolymer systems, 1(a) Pivot algorithm and pair distribution function". *Macromol. Theory Simul.*, **7**(4):381–389, 1998.

[29] Q. Wang, P. F. Nealey, and J. J. de Pablo. "Monte Carlo simulations of asymmetric diblock copolymer thin films confined between two homogeneous surfaces". *Macromolecules*, **34**(10):3458–3470, 2001.

[30] R. H. Swendsen and J. S. Wang. "Replica Monte Carlo simulation of spin-glasses". *Phys. Rev. Lett.*, **57**(21):2607–2609, 1986.

[31] A. M. Ferrenberg and R. H. Swendsen. "Optimized Monte Carlo data analysis". *Phys. Rev. Lett.*, **63**(12):1195–1198, 1989.

[32] M. Muller and N. B. Wilding. "Concentration and energy fluctuations in a critical polymer mixture". *Phys. Rev. E*, **51**(3):2079–2089, 1995.

[33] P.-G. de Gennes. *Scaling Concepts in Polymer Physics*. Cornell University Press, 1979.

[34] http://www.fftw.org.

[35] W. H. Press, S. A. Teukolsky, W. T. Vetterling, and B. P. Flannery. Chap. 9.7 in *Numerical Recipes in C: the Art of Scientific Computing*, 2nd Ed. Cambridge University Press, 2002.

[36] R. B. Thompson, K. O. Rasmussen, and T. Lookman. "Improved convergence in block copolymer self-consistent field theory by Anderson mixing". *J. Chem. Phys.*, **120**(1):31–34, 2004.

[37] Q. Wang. "Effects of interaction range and compressibility on the microphase separation of diblock copolymers: Mean-field analysis". *J. Chem. Phys.*, **129**(5):054904, 2008.

[38] M. W. Matsen. "Self-consistent field theory for melts of low-molecular-weight diblock copolymer". *Macromolecules*, **45**(20):8502–8509, 2012.

[39] F. J. Martinez-Veracoechea and F. A. Escobedo. "Simulation of the gyroid phase in off-lattice models of pure diblock copolymer melts". *J. Chem. Phys.*, **125**(10), 2006.

[40] Q. Wang, P. F. Nealey, and J. J. de Pablo. "Lamellar structures of symmetric diblock copolymers: Comparisons between lattice Monte Carlo simulations and self-consistent mean-field calculations". *Macromolecules*, **35**(25):9563–9573, 2002.

[41] G. H. Fredrickson, V. Ganesan, and F. Drolet. "Field-theoretic computer simulation methods for polymers and complex fluids". *Macromolecules*, **35**(1):16–39, 2002.